Systems/Circuits

Region-Specific and State-Dependent Astrocyte Ca^{2+} Dynamics during the Sleep-Wake Cycle in Mice

Tomomi Tsunematsu,[1,2,3] Shuzo Sakata,[4] Tomomi Sanagi,[2] Kenji F. Tanaka,[5] and Ko Matsui[1]

[1]Super-network Brain Physiology, Graduate School of Life Sciences, Tohoku University, Sendai 980-8577, Japan, [2]Advanced Interdisciplinary Research Division, Frontier Research Institute for Interdisciplinary Sciences, Tohoku University, Sendai 980-8578, Japan, [3]Precursory Research for Embryonic Science and Technology, Japan Science and Technology Agency, Kawaguchi 332-0012, Japan, [4]Strathclyde Institute of Pharmacy and Biomedical Sciences, University of Strathclyde, Glasgow G4 0RE, United Kingdom, and [5]Department of Neuropsychiatry, Keio University School of Medicine, Tokyo 160-8582, Japan

Neural activity is diverse, and varies depending on brain regions and sleep/wakefulness states. However, whether astrocyte activity differs between sleep/wakefulness states, and whether there are differences in astrocyte activity among brain regions remain poorly understood. Therefore, in this study, we recorded astrocyte intracellular calcium (Ca^{2+}) concentrations of mice during sleep/wakefulness states in the cortex, hippocampus, hypothalamus, cerebellum, and pons using fiber photometry. For this purpose, male transgenic mice expressing the genetically encoded ratiometric Ca^{2+} sensor YCnano50 specifically in their astrocytes were used. We demonstrated that Ca^{2+} levels in astrocytes substantially decrease during rapid eye movement (REM) sleep, and increase after the onset of wakefulness. In contrast, differences in Ca^{2+} levels during non-REM (NREM) sleep were observed among the different brain regions, and no significant decrease was observed in the hypothalamus and pons. Further analyses focusing on the transition between sleep/wakefulness states and correlation analysis with the duration of REM sleep showed that Ca^{2+} dynamics differs among brain regions, suggesting the existence of several clusters, i.e., the first comprising the cortex and hippocampus, the second comprising the hypothalamus and pons, and the third comprising the cerebellum. Our study thus demonstrated that astrocyte Ca^{2+} levels change substantially according to sleep/wakefulness states. These changes were consistent in general unlike neural activity. However, we also clarified that Ca^{2+} dynamics varies depending on the brain region, implying that astrocytes may play various physiological roles in sleep.

Key words: **astrocyte; calcium; sleep; wakefulness**

Significance Statement

Sleep is an instinctive behavior of many organisms. In the previous five decades, the mechanism of the neural circuits controlling sleep/wakefulness states and the neural activities associated with sleep/wakefulness states in various brain regions have been elucidated. However, whether astrocytes, which are a type of glial cell, change their activity during different sleep/wakefulness states was poorly understood. Here, we demonstrated that dynamic changes in astrocyte Ca^{2+} concentrations occur in the cortex, hippocampus, hypothalamus, cerebellum, and pons of mice during natural sleep. Further analyses demonstrated that Ca^{2+} dynamics slightly differ among different brain regions, implying that the physiological roles of astrocytes in sleep/wakefulness might vary depending on the brain region.

Introduction

Astrocytes, which are the main subtype of glial cells, are essential for central nervous system development and function. Many previous studies have clarified that astrocytes have housekeeping roles in brain function, contributing to ion and neurotransmitter homeostasis, formation, and maintenance of the blood-brain barrier (Sofroniew and Vinters, 2010; Bojarskaite et al., 2020), regulation of blood flow, metabolic support for neurons (Magistretti and Allaman, 2018), neurotransmitter recycling (Sofroniew and Vinters, 2010), and regulation of synaptogenesis and synaptic transmission (Allen, 2014; Allen and Eroglu, 2017). All of these physiological functions of astrocytes are strongly

Received Nov. 16, 2020; revised Apr. 6, 2021; accepted May 2, 2021.

Author contributions: T.T. designed research; T.T. performed research; K.F.T. contributed unpublished reagents/analytic tools; T.T., S.S., T.S., and K.M. analyzed data; T.T. and S.S. wrote the paper.

This work was supported by the Japan Science and Technology Agency PRESTO Grant JPMJPR1887 and the Japan Society for the Promotion of Science (JSPS) KAKENHI Grant 20H05047 (to T.T.) and by the JSPS Grant-in-Aid for Scientific Research (B) 19H03338, the JSPS Grant-in-Aid for Challenging Exploratory Research 18K19368, and a Toray Science Foundation grant (K.M.). We thank A. Utsumi for assistance with the data analyses, Dr. S. Niwa for technical assistance, and Dr. Helena Akiko Popiel for English language editing of the manuscript.

The authors declare no competing financial interests.

Correspondence should be addressed to Tomomi Tsunematsu at tsune@tohoku.ac.jp.

https://doi.org/10.1523/JNEUROSCI.2912-20.2021

associated with the dynamics of their intracellular calcium (Ca^{2+}) concentration. Intrinsic signals, including those involving neurotransmitters, protons, cannabinoids, polyphosphate, and endothelin result in increases in astrocyte Ca^{2+} concentrations (Gourine et al., 2010; Navarrete and Araque, 2010; Filosa et al., 2012; Min and Nevian, 2012; Holmström et al., 2013). In turn, the activated astrocytes release neuroactive substances called gliotransmitters, which activate neurons and vascular smooth muscle (Sasaki et al., 2012; Araque et al., 2014; Beppu et al., 2014; Savtchouk and Volterra, 2018).

In addition, it has become clear that astrocytes are involved in the regulation and physiological functions of mammalian sleep (Frank, 2019). There is evidence that astrocytes regulate sleep pressure through soluble *N*-ethylmaleimide-sensitive factor attachment protein receptor (SNARE)-dependent adenosine release (Halassa et al., 2009; Florian et al., 2011). Astrocytes also promote the sleep-dependent clearance of brain waste products, such as β-amyloid (Xie et al., 2013). The dysfunction of gap junctions in astrocytes leads to the inability to transfer lactate to wake-promoting orexin neurons in the lateral hypothalamic area, resulting in sleep disorders (Clasadonte et al., 2017), whereas optogenetic stimulation of astrocytes in the hypothalamus increases sleep (Pelluru et al., 2016). Furthermore, astrocytes also regulate cortical state switching (Poskanzer and Yuste, 2016). These results strongly indicate that astrocytes play a pivotal role in sleep as well as other brain functions.

However, astrocytic Ca^{2+} dynamics in natural sleep has been poorly understood, although an imaging study demonstrated that general anesthesia disrupts astrocyte Ca^{2+} signaling in mice (Thrane et al., 2012). Recent studies have recorded astrocyte Ca^{2+} changes during sleep/wakefulness in mice, but to date, data have only been reported for the cortex (Bojarskaite et al., 2020; Ingiosi et al., 2020). Accumulating evidence has shown that astrocytes are heterogeneous with respect to their transcriptomes and functions among various brain regions as well as among various neuronal types (Chai et al., 2017; Morel et al., 2017; Zeisel et al., 2018; Batiuk et al., 2020; Bayraktar et al., 2020; Lozzi et al., 2020). It is well known that neurons in various brain regions, i.e., the hypothalamus, midbrain, and brainstem, control the sleep/wakefulness state, as well as rapid eye movement (REM)/non-REM (NREM) sleep, via a flip-flop circuit. (Sakurai, 2007; Weber and Dan, 2016; Scammell et al., 2017; Liu and Dan, 2019). However, little is known about how astrocyte Ca^{2+} concentrations in brain regions other than the cortex change depending on the sleep/wakefulness state, and whether there are dynamic differences in astrocyte Ca^{2+} levels among the different brain regions. Therefore, in this study, we performed fiber photometry recordings of astrocyte Ca^{2+} dynamics of the cerebellum, cortex, hippocampus, hypothalamus, and pons of mice during the sleep-wake cycle. To optically record astrocyte Ca^{2+} dynamics, we used megalencephalic leukoencephalopathy with subcortical cysts 1 (*Mlc1*)-tetracygline transactivator (tTA); TetO-YCnano50 bigenic mice (Horikawa et al., 2010; Tanaka et al., 2010, 2012; Kanemaru et al., 2014) in which astrocytes specifically express YCnano50.

In this study, we demonstrated that astrocyte Ca^{2+} levels consistently decrease during REM sleep, and immediately increase with the onset of wakefulness. In contrast, differences in Ca^{2+} levels during NREM sleep were observed in various brain regions. There was a significant decrease in Ca^{2+} levels in the cerebellum, cortex, and hippocampus during NREM sleep, but no significant decrease was observed in the hypothalamus and pons.

Materials and Methods

Animals

All experimental procedures involving animals were approved by the Animal Care and Use Committee of Tohoku University (approval no. 2019LsA-018) and were conducted in accordance with the National Institute of Health guidelines. All efforts were made to minimize animal suffering and discomfort, and to reduce the number of animals used. *Mlc1*-tTA; TetO-YCnano50 mice, which were used to monitor the dynamics of intracellular calcium concentration in astrocytes, were produced by crossing *Mlc1*-tTA mice (Tanaka et al., 2010) with TetO-YCnano50 mice (Kanemaru et al., 2014). The following PCR primer sets were used for mouse genotyping: MlcU-675 (5′-AAATTCAGGAA GCTGTGTGCCTGC-3′) and mtTA24L (5′-CGGAGTTGATCACCTT GGACTTGT-3′) for *Mlc1*-tTA mice; and tetO-up (5′-AGCAGAGCTC GTTTAGTGAACCGT-3′) and intron-low (5′-AAGGCAGGATGAT GACCAGGATGT-3′) for TetO-YCnano50 mice. Mice were housed under a controlled 12 h/12 h light/dark cycle (light on hours 8:30 A.M. to 8:30 P.M.). Mice had *ad libitum* access to food and water. A total of 14 male mice (nine *Mlc1*-tTA; TetO-YCnano50 mice and five *Mlc1*-tTA mice as controls) were used in this study. The following number of mice were used for the recording of each brain area: cerebellum, three mice (five recordings); cortex, three mice (six recordings); hippocampus, one mouse (two recordings); hypothalamus, two mice (four recordings); pons, one mouse (two recordings). For the recording of control *Mlc1*-tTA mice, three mice were used (eight recordings). For the freely moving recording, two *Mlc1*-tTA; TetO-YCnano50 mice and two *Mlc1*-tTA mice as controls were used.

Surgical procedures

Male *Mlc1*-tTA; TetO-YCnano50 bigenic mice and *Mlc1*-tTA monogenic mice ($\geq$12 weeks of age) were used. Stereotaxic surgery was performed under anesthesia with pentobarbital (5 mg/kg, i.p. as induction) and with isoflurane (1–2% for maintenance) using a vaporizer for small animals (Bio Research Center) with the mice positioned in a stereotaxic frame (Narishige). Two bone screws were implanted on the skull as electrodes for cortical electroencephalograms (EEGs), and twisted wires (AS633, Cooner Wire) were inserted into the neck muscle as an electrode for electromyograms (EMGs). Another bone screw was implanted in the cerebellum as a ground. All electrodes were connected to a pin socket.

For fiber photometry experiments, a cannula (CF440-10, Thorlabs) with a glass optical fiber (φ 400 μm, 0.39 NA, Thorlabs) was implanted into the cortex (1.2 mm posterior, 3.1 mm lateral from bregma, 0.3 mm depth from the brain surface), hippocampus (1.7 mm posterior, 1.5 mm lateral from bregma, 1.3 mm depth from the brain surface), hypothalamus (1.8 mm posterior, 1.0 mm lateral from bregma, 4.5 mm depth from the brain surface), cerebellum (6.0 mm posterior, 1.0 mm lateral from bregma, and 0.5 mm depth from the brain surface), and pons (5.1 mm posterior, 1.2 mm lateral from bregma, and 3.5 mm depth from the brain surface). All electrodes and optical fiber cannulas were fixed to the skull with dental cement. To fixate the head of mice, a stainless chamber frame (CF-10, Narishige) was also attached to the skull using dental cement. After the surgery, the mice were left to recover for at least 5 d. During the habituation period, mice were placed in a head-fix apparatus (MAG-1, Narishige), by securing them by the stainless chamber frame and placing them into an acrylic tube. This procedure was continued for at least 5 d, during which the duration of head-fixation was gradually extended from ten to 120 min.

In vivo fiber photometry experiments in the head-fixed condition

To detect the dynamics of intracellular Ca^{2+} concentrations in astrocytes, a fiber photometric system (Lucir) was used. A 420 nm violet light-emitting diode (LED; Doric) was used to obtain Ca^{2+}-dependent signals. Recording in the head-fixed condition was performed for about 5 h/d. During recording, EEGs and EMGs were recorded continuously, whereas excitation light (20 Hz, 5 ms in width) was intermittently illuminated at random for 4 min each time. The input light was reflected off a dichroic mirror (FF458-Di02, Semrock) coupled to an optical fiber. LED

power was 1.12 ± 0.18 mW/mm^2 at the fiber tip. Light emission of cyan and yellow fluorescence from YCnano50 was collected via an optical fiber cannula, divided by a dichroic mirror (FF509-FDi01, Semrock) into cyan (483/32-nm bandpass filter, Semrock) and yellow (542/27-nm bandpass filter, Semrock), and detected by each photomultiplier (Lucir). Excitation signals were generated by a pulse generator (AWG-50, Elmos) to control the LEDs. Fluorescence data were acquired at a sampling rate of 1 kHz through an analog-to-digital converter [Micro1401-3, Cambridge Electronic Design (CED)]. At the same time as the fluorescence recording, EEG and EMG signals were amplified (DAM50, World Precision Instruments), filtered, and digitized at 1 kHz using an analog-to-digital converter. EEG and EMG signals were high-pass and low-pass filtered at 0.1 and 300 Hz, respectively. Locomotion was induced by pinching the tail with forceps. Data were recorded using Spike2 software (CED).

In vivo sleep/wakefulness recording using freely moving mice

For the analysis of freely moving mice, continuous EEG and EMG recordings were performed through a slip ring (SPM-35-8P-03, HIKARI DENSHI), which was designed so that the movement of the mice was unrestricted. EEG and EMG signals were amplified (AB-610J, Nihon Koden), filtered (EEG, 0.75–20 Hz; EMG, 20–50 Hz), digitized at a sampling rate of 128 Hz, and recorded using SleepSign software version 3 (Kissei Comtec).

Histologic analysis

To confirm the position of the implanted optical fibers, mice were deeply anesthetized with isoflurane and perfused sequentially with 20 ml of chilled saline and 20 ml of chilled 4% paraformaldehyde in phosphate buffer solution (Nacalai Tesque). The brains were removed and immersed in the above fixation solution overnight at 4°C, and then immersed in 30% sucrose in PBS for at least 2 d. The brains were quickly frozen in embedding solution (Sakura Finetek), and cut into coronal sections using a cryostat (CM3050, Leica) at a thickness of 40 and 50 μm. For immunostaining, to confirm the expression of YCnano50 in astrocytes, the brain sections of *Mlc1*-tTA; TetO-YCnano50 bigenic mice were incubated with mouse anti-S100β antibody (1:1000; S2532, Merck) or mouse anti-GFAP antibody (1:2000; G3893, Merck) overnight at 4°C. Then, the sections were incubated with CF594 donkey anti-mouse IgG (1:1000; 20116-1, Nacalai Tesque) for 1 h at room temperature, mounted onto APS-coated slides, coverslipped with 50% glycerol in PBS, and observed using a fluorescence microscope (BZ-9000, Keyence) or a confocal microscope (LSM800, Zeiss).

Data analysis

Sleep scoring

Polysomnographic recordings were automatically scored offline, with each epoch scored as wakefulness, NREM sleep, or REM sleep by SleepSign (Kissei Comtec), in 4-s epochs, according to standard criteria (Radulovacki et al., 1984; Tobler et al., 1997). All vigilance state classifications assigned by SleepSign were confirmed visually. The same individual, blinded to mouse genotype and experimental condition, scored all EEG/EMG recordings. Spectral analysis of the EEGs was performed by fast Fourier transform, which yielded a power spectral profile with a 1-Hz resolution divided into δ (1−5 Hz), θ (6−10 Hz), α (10−13 Hz), β (13−25 Hz), and γ (30−50 Hz) waves. To quantify EMG amplitude, the root-mean-square (rms) was calculated.

Fiber photometry signal processing

In Figures 1-4, axoGraph was used to calculate yellow fluorescence protein (YFP) to cyan fluorescence protein (CFP; Y/C) ratios. The average value of the YFP intensity and CFP intensity for each light illumination (5 ms) was calculated, and then the Y/C ratio was calculated. For the comparison of Y/C ratios during the sleep/wakefulness states, the Y/C ratio of each episode was normalized with the average value during wakefulness set as 1. For sleep/wakefulness state transition analyses, four consecutive epochs (16 s) of one state followed immediately by eight consecutive epochs (32 s) of a distinct state were used. To assess correlations between Y/C ratio and EEG/EMG power (Figs. 2, 4), spectral densities of EEG signals in every 1-s window were estimated at δ (1–5 Hz), θ (6–10 Hz), α (13–25 Hz), β (13–25 Hz), and γ (30–50 Hz) bands using the multitaper method (http://chronux.org/). EMG power was calculated as the common logarithm of a rms value in every 1-s window. The mean of Y/C ratio in the corresponding 1-s window was also calculated. Pearson's correlation coefficient was computed based on z-scored values in each state.

In Figure 5, all data analyses were performed by custom written MATLAB software (MathWorks). To compute normalized Y/C ratios during the time-normalized episodes, Y/C ratios were first normalized by the mean Y/C ratio during wakefulness. To obtain the time-normalized Ca^{2+} dynamics, each episode was segmented into five bins, and the mean Y/C ratio was computed for each bin. Episodes were classified based on vigilance states before and after the episode.

Decoding

To decode sleep/wakefulness states based on Ca^{2+} signals, the same approach as described previously was used (Tsunematsu et al., 2020). Briefly, the mean Y/C ratio was computed in each corresponding window (4 s). After training a linear classifier, classification performance was calculated with fourfold cross validation.

Experimental design and statistical analysis

Data are presented as the mean ± SEM unless otherwise stated. Statistical analyses were performed using MATLAB. Multiple group comparisons were performed by one-way ANOVA in samples with a Gaussian distribution, and by the Kruskal–Wallis test in samples with a non-Gaussian distribution, with the *post hoc* Bonferroni test. In Figure 5*B*, one-way ANOVA with the *post hoc* Tukey's HSD test was performed; p values of <0.05 were considered to indicate a statistically significant difference between groups. To calculate effect size, power analyses were performed using G*Power 3.1 (Faul et al., 2007).

Results

Fiber photometry recording of Ca^{2+} signals in cerebellar astrocytes

To elucidate the dynamics of intracellular Ca^{2+} concentration in astrocytes during sleep/wakefulness states, we used *Mlc1*-tTA; TetO-YCnano50 bigenic mice. Mlc1 is an astrocyte-specific protein with unknown function, which is highly expressed in perivascular astrocyte end-feet and astrocyte-astrocyte contacts (Boor et al., 2005; Teijido et al., 2007). We first focused on cerebellar astrocytes, and investigated the Ca^{2+} changes. It has been reported that the activity of Bergmann glial cells, a specific type of radial astrocyte in the cerebellum, is inhibited in the anesthetized state compared with in the awake state (Hoogland et al., 2009; Nimmerjahn et al., 2009). Therefore, we hypothesized that cerebellar astrocytes may demonstrate state-dependent Ca^{2+} dynamics throughout the sleep-wake cycle. To this end, we took advantage of the strong fluorescence intensity of cerebellar astrocytes in *Mlc1*-tTA; TetO-YCnano50 bigenic mouse line (Kanemaru et al., 2014).

To confirm astrocyte-specific expression of YCnano50 in the cerebellum, we performed immunostaining of astrocytes using S100β, an astrocyte-specific marker. The merged images show that YCnano50 was exclusively observed in cerebellar astrocytes in *Mlc1*-tTA; TetO-YCnano50 bigenic mice, and ectopic expression was not observed (Fig. 1*A*). Astrocytes in the cortex and hippocampus sparsely expressed YCnano50 as previously reported (Kanemaru et al., 2014). In this study, fiber photometry was used to record changes in astrocyte Ca^{2+} concentrations from head-fixed mice, as Y/C ratios (Fig. 1*B*). We first confirmed whether Y/C ratios calculated from the YFP fluorescence and CFP fluorescence precisely reflect the changes in astrocyte Ca^{2+} concentrations under our experimental conditions. For this

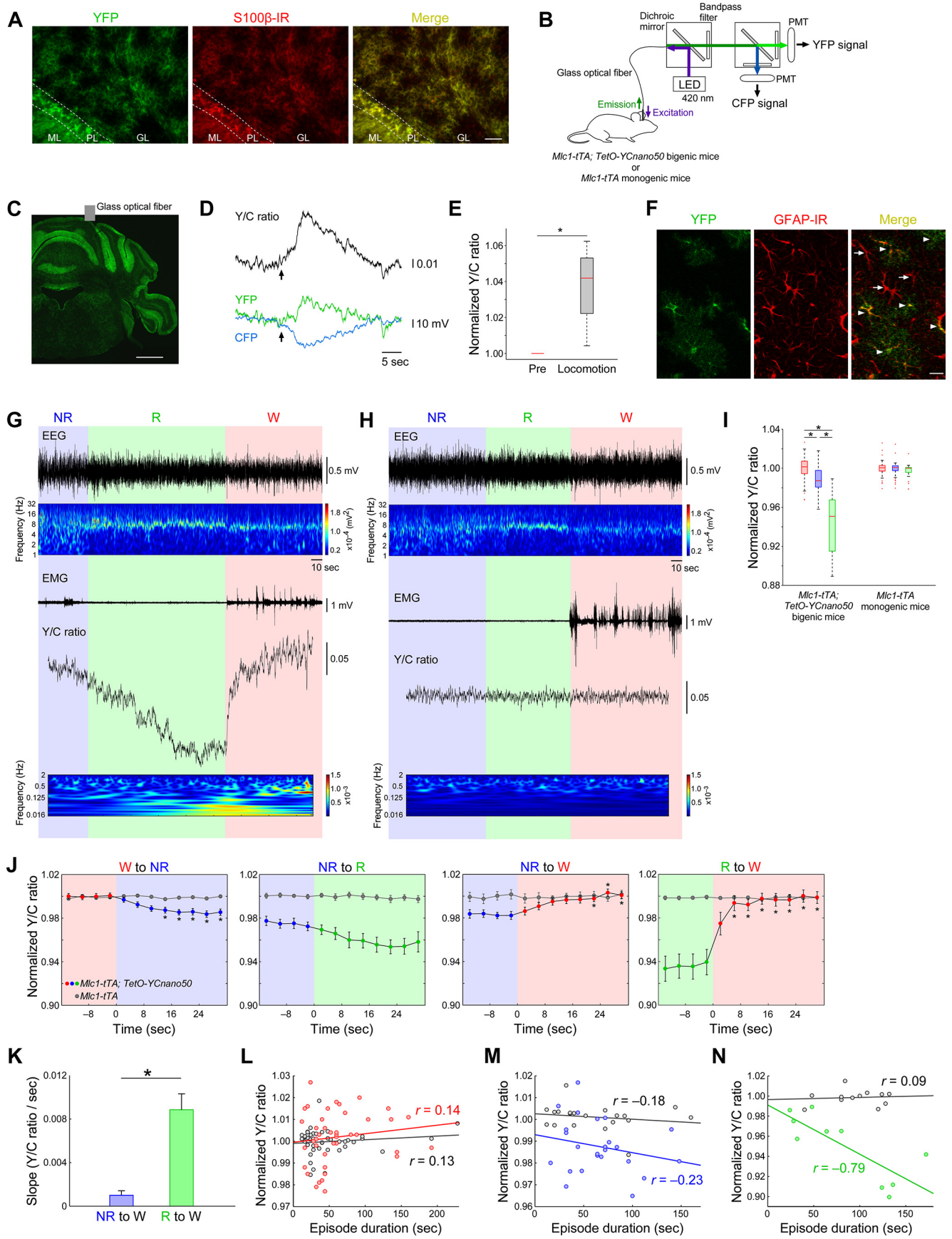

Figure 1. Astrocyte Ca^{2+} dynamics in the cerebellum during sleep/wakefulness states of mice. ***A***, Immunohistochemical analysis demonstrating that YCnano50 is specifically expressed in cerebellar astrocytes in the *Mlc1*-tTA; TetO-YCnano50 bigenic mouse brain. Left, YFP fluorescence of YCnano50-positive cells (green). Middle, S100β-immunoreactive astrocytes (red). Left, Merged image (yellow). Scale bar: 40 μm. GL, granule cell layer; ML, molecular layer; PL, Purkinje cell layer. ***B***, Schematic drawing showing the fiber photometry system used in this study.

purpose, we analyzed changes in the Y/C ratio during tail pinch-induced locomotion in mice, as it has previously been reported that astrocyte Ca^{2+} concentrations increase with locomotion and the startle response in mice (Nimmerjahn et al., 2009; Srinivasan et al., 2015; Bojarskaite et al., 2020). To deliver excitation light and collect fluorescence signals from the cerebellum, a glass optical fiber was implanted into the cerebellum of mice (Fig. 1*C*). Immediately after the tail pinch-induced locomotion, YFP fluorescence and CFP fluorescence showed changes in opposite directions, resulting in an increase in the Y/C ratio (Fig. 1*D*). The average Y/C ratio of the 10 s immediately before the tail pinch-induced locomotion was set to 1. The average Y/C ratio of the 10 s immediately after the tail pinch-induced locomotion was normalized, and a significant increase in Y/C ratio on locomotion was observed ($n = 4$ from three recording sessions and one animal; paired t test, $^*p < 0.05$).

To assess the effect of YCnano50 expression in astrocytes, we examined whether there are any signs of reactive astrocyte. We compared with the hippocampal astrocytes which have sparce expression of YCnano50. There was no morphologic change and no signs of upregulation of glial fibrillary acidic protein (GFAP) immunoreactivity between YCnano50-expressing astrocytes and intact astrocytes (Fig. 1*F*), indicating no toxic effects. To further confirm the effect of YCnano50 expressed in bigenic mouse astrocytes and the effect of the head-fixed condition on sleep architecture, we compared the duration of each sleep/wakefulness episode and time spent in each sleep/wakefulness state during the light period (9 A.M. to 3 P.M.) between the mice. To determine the sleep/wakefulness state of mice, EEG and EMG electrodes were implanted into their skulls and neck muscles. There were no significant differences between *Mlc1*-tTA; TetO-YCnano50 bigenic mice (six recording sessions and two animals) and *Mlc1*-tTA monogenic mice in the freely moving condition [six recording sessions and two animals; episode duration of wakefulness: Kruskal–Wallis: $F_{(3,28)} = 180.9$, $p = 0.10$, no significant difference (NS); episode duration of NREM: Kruskal–Wallis: $F_{(3,28)} = 495.6$, $p < 0.05$, followed by multiple comparisons by the Bonferroni test: $p = 1$, NS; episode duration of REM: Kruskal–Wallis: $F_{(3,21)} = 92.2$, $p = 0.16$, NS; time spent in wakefulness: Kruskal–Wallis: $F_{(3,28)} = 11.1$, $p = 0.94$, NS; time spent in NREM: Kruskal–Wallis: $F_{(3,28)} = 23.1$, $p = 0.85$, NS; time spent in REM: Kruskal–Wallis: $F_{(3,28)} = 112.6$, $p = 0.27$, NS; Table 1]. On the other hand, the episode duration of NREM sleep was significantly reduced in mice in the head-fixed condition (without hypothalamus, 16 recording sessions and six animals) compared with mice in the freely moving condition (six recording sessions and two animals; episode duration of NREM: Kruskal–Wallis: $F_{(3,28)} = 495.6$, $p < 0.05$, followed by multiple comparisons by the Bonferroni test: $p < 0.05$; Table 1). However, no significant differences were observed between the other conditions.

State-dependent Ca^{2+} dynamics in cerebellar astrocytes

We next analyzed the dynamics of intracellular Ca^{2+} concentration in astrocytes during sleep/wakefulness states. Ca^{2+} signal dynamics were recorded during the light period (9 A.M. to 3 P.M.). Excitation light (20 Hz, 5 ms in width) was intermittently illuminated at random for 4 min. Y/C ratios gradually decreased during sleep, showing the lowest value during REM sleep, and instantaneously increased with awakening in *Mlc1*-tTA; TetO-YCnano50 mice (Fig. 1*G*). A decrease in Y/C ratio represents a decrease in Ca^{2+} concentration, as we have previously reported (Natsubori et al., 2017; Tsutsui-Kimura et al., 2017; Yoshida et al., 2020). In contrast, Y/C ratios did not change with sleep/wakefulness state in control *Mlc1*-tTA mice (Fig. 1*H*). The spectrogram of Y/C ratio in *Mlc1*-tTA; TetO-YCnano50 mice exhibited state-dependent changes at below ~0.25 Hz, whereas small fluctuations at above ~0.25 Hz appeared even in Mlc1-tTA mice. These results indicate that signals below ~0.25 Hz reflect state-dependent Ca^{2+} signals in astrocyte. Normalized Y/C ratios in wakefulness, NREM sleep, and REM sleep in cerebellar astrocytes of *Mlc1*-tTA; TetO-YCnano50 mice were 1.000 ± 0.001 ($n = 66$ episodes from 5 recording sessions and 3 animals), 0.988 ± 0.002 ($n = 63$ episodes from 5 recording sessions and three animals), and 0.944 ± 0.008 ($n = 17$ episodes from three recording sessions and 2 animals), respectively (Kruskal–Wallis: $F_{(2,143)} = 56.68$, $p < 0.05$, followed by multiple comparison by the Bonferroni test: $p < 0.05$, effect size f = 1.07; Fig. 1*I*). In contrast, normalized Y/C ratios during wakefulness, NREM sleep, and REM sleep in cerebellar astrocytes of *Mlc1*-tTA mice were 1.000 ± 0.001 ($n = 60$ episodes from 5 recording sessions and 3 animals), 1.000 ± 0.001 ($n = 70$ episodes from 5 recording sessions and three animals), and 0.997 ± 0.001 ($n = 33$ episodes from 5 recording sessions and three animals), respectively (Kruskal–Wallis: $F_{(2,160)} = 4.04$, $p = 0.13$, NS, effect size f = 0.17; Fig. 1*I*). These results indicate that Ca^{2+} concentrations of cerebellar astrocytes change substantially with sleep/wakefulness state in mice.

We next focused on Ca^{2+} dynamics during the transition between sleep/wakefulness states (Fig. 1*J*). Y/C ratios gradually decreased after the onset of NREM sleep following wakefulness. Sixteen seconds after the start of NREM sleep, Y/C ratios significantly decreased compared with when mice were awake ($n = 26$ episodes from three recording sessions and two animals; one-way ANOVA: $F_{(11,300)} = 6.79$, $p < 0.05$, followed by multiple comparisons by the Bonferroni test: $p < 0.05$ vs the fourth epoch immediately before state transition). A slow decrease in Y/C ratios was also observed in the transition from NREM sleep to REM sleep, but there was no significant difference ($n = 10$

←

Fluorescence emission is applied from the LED light source. Yellow and cyan fluorescence signals were corrected by bandpass filters and enhanced by photomultipliers (PMT). ***C***, The location of the glass optical fiber, which was implanted in the cerebellum of *Mlc1*-tTA; TetO-YCnano50 bigenic mice (6.0 mm posterior, 1.0 mm lateral from bregma, 0.5 mm depth from the brain surface). Scale bar: 1 mm. ***D***, Example of Y/C ratios (top) and corresponding intensity changes of yellow and cyan fluorescence (bottom) recorded during tail pinch-induced locomotion in *Mlc1*-tTA; TetO-YCnano50 bigenic mice. The arrows indicate the timing of the tail pinch. ***E***, Box plot summarizing the data from ***D***. The Y/C ratios during locomotion were normalized using the Y/C ratio at 10 s immediately before the locomotion set as 1; $^*p < 0.05$. ***F***, Comparison of GFAP immunoreactivity (red) with (arrowheads) or without (arrows) YCnano50 expression (green) in the hippocampal astrocytes. Scale bar: 15 μm. ***G***, ***H***, Representative traces of EEG, EEG power density spectrum, EMG, cerebellar astrocyte Ca^{2+} signals (Y/C ratio), and Y/C ratio spectrogram in *Mlc1*-tTA; TetO-YCnano50 bigenic mice (***G***) and *Mlc1*-tTA monogenic mice (***H***). ***I***, Box plot summarizing the data from ***G***, ***H***. Y/C ratios were normalized to the value of each episode, with the average value of awakening set as 1; $^*p < 0.05$. ***J***, Y/C ratios during the transitions between the sleep/wakefulness states. Transitions occurred at time 0. Data are from 4-s intervals characterized by state transitions. The line graph with the colored circles and gray circles are a summary of the data from *Mlc1*-tTA; TetO-YCnano50 bigenic mice and *Mlc1*-tTA monogenic mice, respectively; $^*p < 0.05$ versus the fourth epoch immediately before the state transition. ***K***, Bar graph representing the slope of the Y/C ratio of mice at the time of awakening from NREM sleep and REM sleep; $^*p < 0.05$. ***L–N***, Analyses of the correlation between Y/C ratios and episode duration of wakefulness (***L***), NREM sleep (***M***), and REM sleep (***N***). Colored circles and gray circles indicate the summary of data from *Mlc1*-tTA; TetO-YCnano50 bigenic mice and *Mlc1*-tTA monogenic mice, respectively. NR, NREM sleep; R, REM sleep; W, wakefulness. Values are shown as means ± SEM.

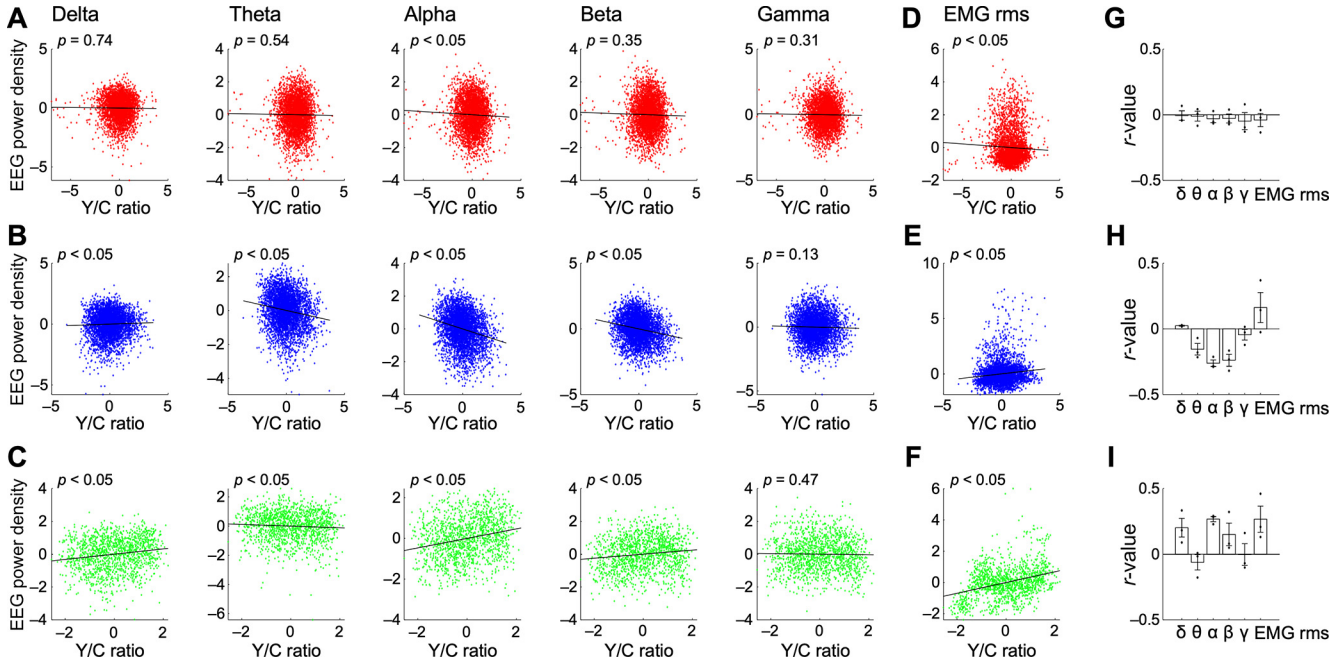

Figure 2. Correlation between EEG/EMG and cerebellar astrocytic Ca^{2+} signals during different sleep/wakefulness states. ***A–C***, Correlation analyses between normalized (z-scored) cerebellar astrocytic Y/C ratios, and normalized (z-scored) EEG power densities in the δ (1–5 Hz), θ (6–10 Hz), α (10–13 Hz), β (13–25 Hz), and γ (30–50 Hz) waves during wakefulness (***A***), NREM sleep (***B***), and REM sleep (***C***). ***D–F***, Correlation analyses between normalized Y/C ratios and normalized rms of EMG during wakefulness (***D***), NREM sleep (***E***), and REM sleep (***F***). The data in this figure were analyzed in 1-s bin sizes. ***G–I***, Bar graphs showing correlation coefficients summarizing the data from ***A–F***. The correlation coefficient of each recording was cross-validated by splitting the data into the first and second halves. Values are shown as means ± SEM.

Table 1. Sleep architecture in mice in the head-fixed condition and freely moving condition

	Wakefulness	NREM	REM
Episode duration (s)			
Free-moving condition of Mlc1-tTA mice	158.7 ± 25.5	187.3 ± 14.9	87.8 ± 14.5
Free-moving condition of Mlc1-tTA; TetO-YCnano50 mice	197.0 ± 24.6	205.8 ± 18.7	62.3 ± 6.0
Head-fixed condition without recording from hypothalamus of Mlc1-tTA; TetO-YCnano50 mice	134.6 ± 32.7	105.7 ± 18.4*	90.9 ± 7.5
Head-fixed condition with recording from hypothalamus of Mlc1-tTA; TetO-YCnano50 mice	102.1 ± 36.9	106.3 ± 13.8	86.8 ± 26.4
Time spent in each state (%)			
Freely moving condition of Mlc1-tTA mice	42.6 ± 4.9	52.2 ± 3.4	5.2 ± 1.1
Freely moving condition of Mlc1-tTA; TetO-YCnano50 mice	46.6 ± 3.1	49.5 ± 2.7	3.9 ± 0.9
Head-fixed condition without recording from hypothalamus	48.4 ± 6.2	43.4 ± 5.1	8.2 ± 1.5
Head-fixed condition with recording from hypothalamus	41.9 ± 7.4	51.6 ± 5.2	6.5 ± 3.4

Data are shown as means ± SD.
*$p < 0.05$, head-fixed condition without recording from hypothalamus versus freely moving condition of *Mlc1*-tTA mice and freely moving condition of *Mlc1*-tTA; TetO-YCnano50 mice.

episodes from two recording sessions and two animals; one-way ANOVA: $F_{(11,108)} = 2.35$, $p < 0.05$, followed by multiple comparison by the Bonferroni test: $p \geq 0.05$, NS). During the transition from NREM and REM sleep to wakefulness, the Y/C ratio increased (from NREM to wakefulness: $n = 19$ episodes from four recording sessions and three animals; from REM to wakefulness: $n = 14$ episodes from three recording sessions and two animals; from NREM to wakefulness, one-way ANOVA: $F_{(11,216)} = 5.47$, $p < 0.05$, followed by multiple comparisons by the Bonferroni test: $p < 0.05$ vs the fourth epoch immediately before state transition; from REM to wake, one-way ANOVA: $F_{(11,156)} = 12.87$, $p < 0.05$, followed by multiple comparisons by the Bonferroni test: $p < 0.05$ vs the fourth epoch immediately before state transition). However, the slopes were completely different between from NREM to wakefulness and from REM to wakefulness. The slope was calculated by dividing the difference in Y/C ratios immediately before and after the transition by 4 s. The slope from REM to wakefulness ($n = 14$ episodes from three recording sessions and two animals) was significantly larger than the slope from NREM to wakefulness ($n = 19$ episodes from four recording sessions and 3 animals; unpaired t test, $p < 0.05$; Fig. 1*K*). These results indicate that the signaling pathway that increases intracellular Ca^{2+} concentrations might differ between from REM sleep and from NREM sleep, although they do not appear to precede the 4-s bin.

Next, correlation analysis was performed to investigate the association between the episode duration of wakefulness, NREM, and REM, and changes in Ca^{2+} concentrations (Fig. 1*L–N*). There was no significant correlation between wakefulness and NREM sleep in either *Mlc1*-tTA; TetO-YCnano50 mice (wakefulness: $n = 41$ episodes from three recording sessions and two animals; NREM: $n = 24$ episodes from three recording sessions and two animals; wakefulness: $r = 0.14$, $p = 0.38$, NS; NREM: $r = -0.23$, $p = 0.28$, NS) or in *Mlc1*-tTA mice (wakefulness: $n = 46$ episodes from five recording sessions and three animals; NREM: $n = 20$ episodes from four recording sessions and three animals; wakefulness: $r = 0.13$, $p = 0.40$, NS; NREM: $r = -0.18$, $p = 0.45$, NS; Fig. 1*L*,*M*). In contrast, there was a significant negative

correlation between the episode duration of REM and Y/C ratio in *Mlc1*-tTA; TetO-YCnano50 mice ($n = 10$ episodes from two recording sessions and two animals; $r = -0.79$, $p < 0.05$; Fig. 1*N*), which is in good agreement with the gradual decrease in Ca^{2+} level during REM sleep. On the other hand, no significant correlation was observed in *Mlc1*-tTA mice ($n = 12$ episodes from two recording sessions and two animals; $r = 0.09$, $p = 0.79$, NS; Fig. 1*N*). These results indicate that Ca^{2+} concentration in cerebellar astrocytes decreases as REM sleep episode duration increases.

Correlation between EEG/EMG and Ca^{2+} signals in cerebellar astrocytes during sleep/wakefulness

Our results up to this point demonstrated that cerebellar astrocyte Ca^{2+} concentrations change dynamically with sleep/wakefulness state. Therefore, we next investigated whether Ca^{2+} fluctuations in cerebellar astrocytes also correlate with electrophysiological features during each sleep/wakefulness state. For this purpose, we investigated the association between Y/C ratios and cortical EEGs and EMGs during wakefulness, NREM, and REM sleep (50 recording sessions and three animals). Cortical EEGs were analyzed by dividing them into δ (1–5 Hz), θ (6–10 Hz), α (10–13 Hz), β (13–25 Hz), and γ (30–50 Hz) wave components. Regarding EMGs, their magnitudes were evaluated by calculating the rms. Then, their correlation with Y/C ratios was analyzed. During wakefulness, although Y/C ratios showed a significant negative correlation with α waves and EMG rms (Fig. 2*A*,*D*), the effect was weak (Fig. 2*G*), suggesting little cofluctuation of Ca^{2+} and electrophysiological signals during wakefulness. A negative correlation between EMG rms and Y/C ratio imply that Y/C ratio does not reflect simple motion-related signals. During NREM sleep, Y/C ratios were positively correlated with δ waves and EMG rms, and negatively correlated with θ, α, and β waves (Fig. 2*B*,*E*,*H*). During REM sleep, however, Y/C ratios demonstrated a positive correlation with δ, α, and β waves and EMG rms, and a negative correlation with θ waves (Fig. 2*C*,*F*,*I*). Although this correlation analysis demonstrated significant differences, no highly positive nor highly negative correlation was identified. A minor but statistically significant correlation between cerebellar astrocyte Ca^{2+} concentrations and electrophysiological features, particularly during sleep, was identified.

State-dependent astrocyte Ca^{2+} dynamics among various brain regions

We next assessed whether state-dependent changes in astrocyte Ca^{2+} concentrations are observed not only in the cerebellum but also in other brain regions, and whether the dynamics differ depending on the brain region. Fiber photometry recordings were performed using a glass optical fiber from the cortex and hippocampus, which have been reported to show diversity in neural activity corresponding to the sleep/wakefulness state (Vyazovskiy et al., 2009; Grosmark et al., 2012; Watson et al., 2016; Niethard et al., 2017), and from the hypothalamus and pons, which play a crucial role in the regulation of sleep/wakefulness (Sakurai, 2007; Tsunematsu et al., 2014; Hayashi et al., 2015; Weber et al., 2015; Weber and Dan, 2016; Scammell et al., 2017), using *Mlc1*-tTA; TetO-YCnano50 mice. To deliver excitation light and collect fluorescence signals, a glass optical fiber was implanted into the brains of mice (Fig. 3*A*). Hypothalamic recording of fiber-implanted in head-fixed *Mlc1*-tTA; TetO-YCnano50 mice (four recording sessions and two animals) demonstrated no differences in sleep/wakefulness architecture compared with recordings from other brain regions in head-fixed *Mlc1*-tTA; TetO-YCnano50 mice (16 recording sessions and six animals), although the implanted optical fiber damages the brain and causes similar to glial scarring around the optical fiber (episode duration of wakefulness: Kruskal–Wallis: $F_{(3,28)} = 180.9$, $p = 0.10$, NS; episode duration of NREM: Kruskal–Wallis: $F_{(3,28)} = 495.6$, $p < 0.05$, followed by multiple comparisons by the Bonferroni test: $p = 1$, NS; episode duration of REM: Kruskal–Wallis: $F_{(3,21)} = 92.2$, $p = 0.16$, NS; time spent in wakefulness: Kruskal–Wallis: $F_{(3,28)} = 11.1$, $p = 0.94$, NS; time spent in NREM: Kruskal–Wallis: $F_{(3,28)} = 23.1$, $p = 0.85$, NS; time spent in REM: Kruskal–Wallis: $F_{(3,28)} = 112.6$, $p = 0.27$, NS; Table 1). Interestingly, astrocyte Ca^{2+} levels dynamically changed depending on the sleep/wakefulness state throughout the brain regions that were monitored, and significantly decreased in all areas during REM sleep [$n = 69$ wakefulness (W), 68 NREM sleep (NR), and 25 REM sleep (R) episodes from five recording sessions and three animals in the cortex; $n = 23$ (W), 24 (NR), and 8 (R) episodes from two recording sessions and one animal in the hippocampus; $n = 60$ (W), 69 (NR), and 20 (R) episodes from four recording sessions and two animals in the hypothalamus; $n = 40$ (W), 43 (NR), and 34 (R) episodes from two recording sessions and one animal in the pons; Kruskal–Wallis: $F_{(2,159)} = 29.3$, $p < 0.05$, effect size f = 0.47 in the cortex; Kruskal–Wallis: $F_{(2,52)} = 39.1$, $p < 0.05$, effect size f = 1.34 in the hippocampus; Kruskal–Wallis: $F_{(2,146)} = 30.0$, $p < 0.05$, effect size f = 0.80 in the hypothalamus; Kruskal–Wallis: $F_{(2,114)} = 55.8$, $p < 0.05$, effect size f = 1.13 in the pons, followed by multiple comparisons by the Bonferroni test: $p < 0.05$; Fig. 3*B*]. However, significant decreases in Y/C ratios during NREM sleep were observed in the cortex and hippocampus compared with that during wakefulness. In contrast, in the hypothalamus and pons, no significant differences were observed between the Y/C ratios during wakefulness and NREM sleep, but Y/C ratios were significantly reduced during REM sleep compared with during NREM sleep. These results suggest that astrocyte Ca^{2+} levels are at a minimum during REM sleep, whereas they are high during wakefulness. This trend is consistent with that observed in the cerebellum. On the other hand, Ca^{2+} dynamics during NREM sleep vary depending on the brain region.

Further analyses during the sleep/wakefulness state transition clarified the variety of Ca^{2+} dynamics among the different brain regions (Fig. 3*C*). Focusing on the transition from wakefulness to NREM sleep, no significant changes were seen in the cortex, hypothalamus, and pons ($n = 44$ episodes from six recording sessions and three animals in the cortex; $n = 38$ episodes from two recording sessions and one animal in the hypothalamus; $n = 17$ episodes from one recording session and one animal in the pons; Kruskal–Wallis: $F_{(11,516)} = 11.7$, $p = 0.39$, NS in the cortex; Kruskal–Wallis: $F_{(11,444)} = 3.2$, $p = 0.99$, NS in the hypothalamus; Kruskal–Wallis: $F_{(11,192)} = 7.3$, $p = 0.77$, NS in the pons). However, Y/C ratios gradually decreased in the hippocampus, and the difference became statistically significant after 24 s from state transition ($n = 12$ episodes from two recording sessions and one animal in the hippocampus; Kruskal–Wallis: $F_{(11,132)} = 49.2$, $p < 0.05$, followed by multiple comparisons by the Bonferroni test: $p < 0.05$ vs the fourth epoch immediately before state transition in the hippocampus). A slow decrease in Y/C ratios in the hypothalamus and pons was observed from NREM to REM sleep ($n = 6$ episodes from two recording sessions and one animal in the hypothalamus; $n = 8$ episodes from two recording sessions and one animal in the pons; Kruskal–Wallis: $F_{(11,60)} = 39.9$, $p < 0.05$ in the hypothalamus; Kruskal–Wallis: $F_{(11,84)} = 57.8$,

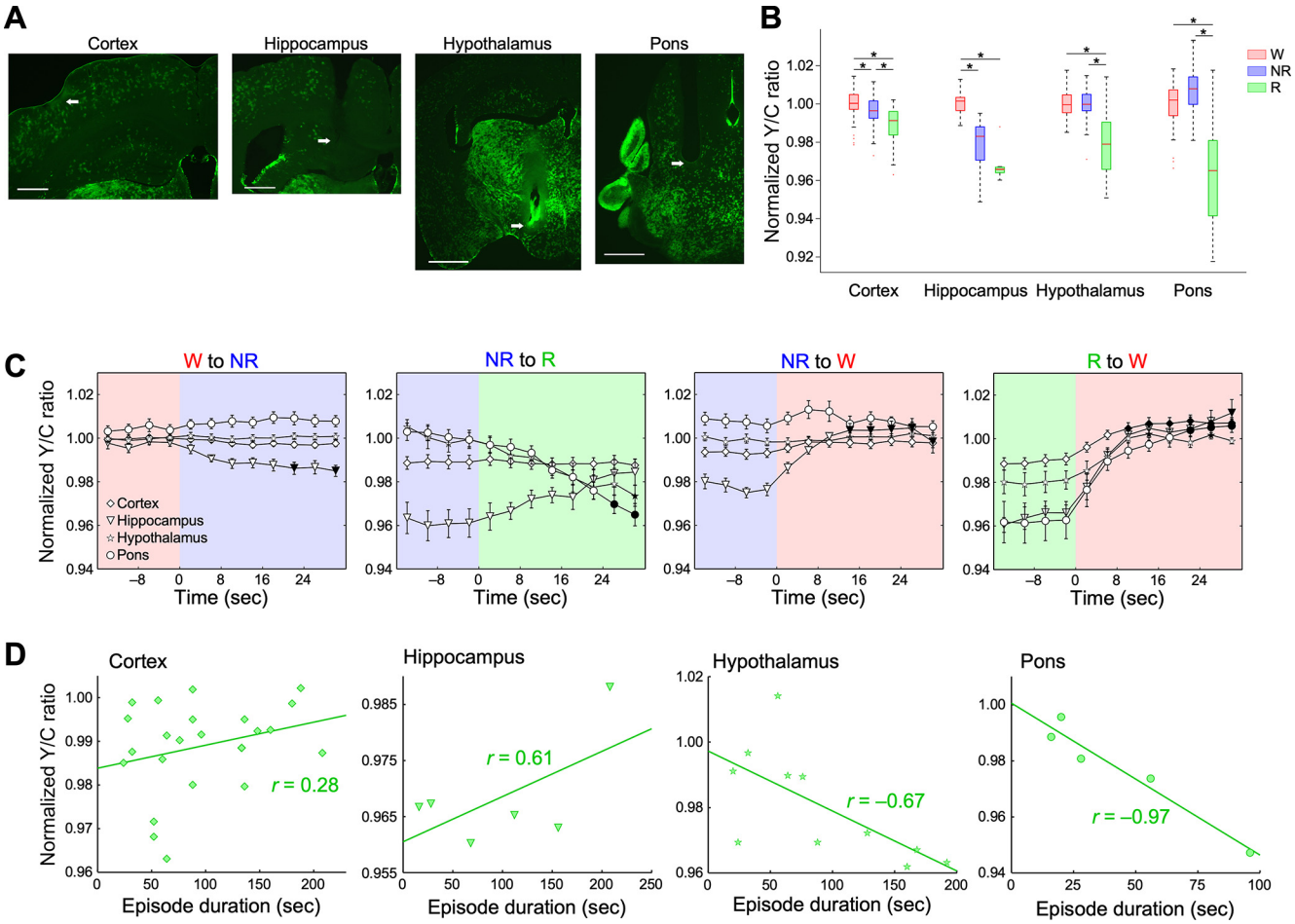

Figure 3. Astrocyte Ca^{2+} dynamics during different sleep/wakefulness states in various brain regions. ***A***, Images indicating the location of the glass optical fiber, which was implanted into the cortex, hippocampus, hypothalamus, and pons. Arrows indicates the tip of the optical fiber. Scale bar: 500 μm (cortex and hippocampus) and 1 mm (hypothalamus and pons). ***B***, Box plot summarizing the data of the normalized Y/C ratios obtained from the cortex, hippocampus, hypothalamus, and pons; $*p < 0.05$. ***C***, Y/C ratios for the transition of sleep/wakefulness states in multiple brain regions. Black filled symbols indicate $p < 0.05$ versus the fourth epoch immediately before state transition in each brain region. ***D***, Correlation analyses between episode durations of REM sleep and Y/C ratios in the cortex, hippocampus, hypothalamus, and pons. NR, NREM sleep; R, REM sleep; W, wakefulness. Values are represented as means ± SEM.

$p < 0.05$ in the pons, followed by multiple comparisons by the Bonferroni test: $p < 0.05$ vs the fourth epoch immediately before state transition), whereas it was almost constant in the cortex but was increased in the hippocampus ($n = 15$ episodes from fix recording sessions and three animals in the cortex; $n = 5$ episodes from two recording sessions and one animal in the hippocampus; Kruskal–Wallis: $F_{(11,168)} = 0.98$, $p = 0.99$, NS in the cortex; Kruskal–Wallis: $F_{(11,48)} = 23.4$, $p < 0.05$, followed by multiple comparisons by the Bonferroni test: NS vs the fourth epoch immediately before state transition in the hippocampus). At the time of transition from NREM sleep to wakefulness, Y/C ratios increased in the hippocampus ($n = 12$ episodes from 2 recording sessions and 1 animal in the hippocampus; Kruskal–Wallis: $F_{(11,132)} = 89.3$, $p < 0.05$, followed by multiple comparisons by the Bonferroni test: $p < 0.05$ vs the fourth epoch immediately before state transition in the hippocampus), but there was no significant difference in the cortex, hypothalamus, and pons ($n = 34$ episodes from seven recording sessions and three animals in the cortex; $n = 25$ episodes from two recording sessions and one animal in the hypothalamus; $n = 7$ episodes from one recording session and one animal in the pons; Kruskal–Wallis: $F_{(11,396)} = 31.8$, $p < 0.05$, followed by multiple comparisons by the Bonferroni test: NS vs the fourth epoch immediately before state transition in the cortex; Kruskal–Wallis: $F_{(11,288)} = 6.0$, $p = 0.87$, NS in the hypothalamus; Kruskal–Wallis: $F_{(11,72)} = 5.4$, $p = 0.91$, NS in the pons). There were consistent increases immediately after the state change from REM sleep to wakefulness in all brain regions that were monitored ($n = 20$ episodes from six recording sessions and three animals in the cortex; $n = 6$ episodes from two recording sessions and one animal in the hippocampus; $n = 12$ episodes from two recording sessions and one animal in the hypothalamus; $n = 12$ episodes from two recording sessions and one animal in the pons; Kruskal–Wallis: $F_{(11,228)} = 109.5$, $p < 0.05$ in the cortex; Kruskal–Wallis: $F_{(11,60)} = 55.5$, $p < 0.05$ in the hippocampus; Kruskal–Wallis: $F_{(11,132)} = 46.8$, $p < 0.05$ in the hypothalamus; Kruskal–Wallis: $F_{(11,132)} = 61.2$, $p < 0.05$ in the pons, followed by multiple comparisons by the Bonferroni test: $p < 0.05$ vs the fourth epoch immediately before state transition).

We also performed correlation analysis to investigate the association between episode duration of REM and changes in Ca^{2+} concentration among the brain regions (Fig. 3*D*). Changes in cortical and hippocampal Y/C ratios were not found to correlate with episode duration of REM sleep ($n = 22$ episodes from six recording sessions and three animals in the cortex; $n = 6$ episodes from two recording sessions and one animal in the hippocampus; $r = 0.28$, $p = 0.21$, NS in the cortex; $r = 0.61$, $p = 0.20$, NS

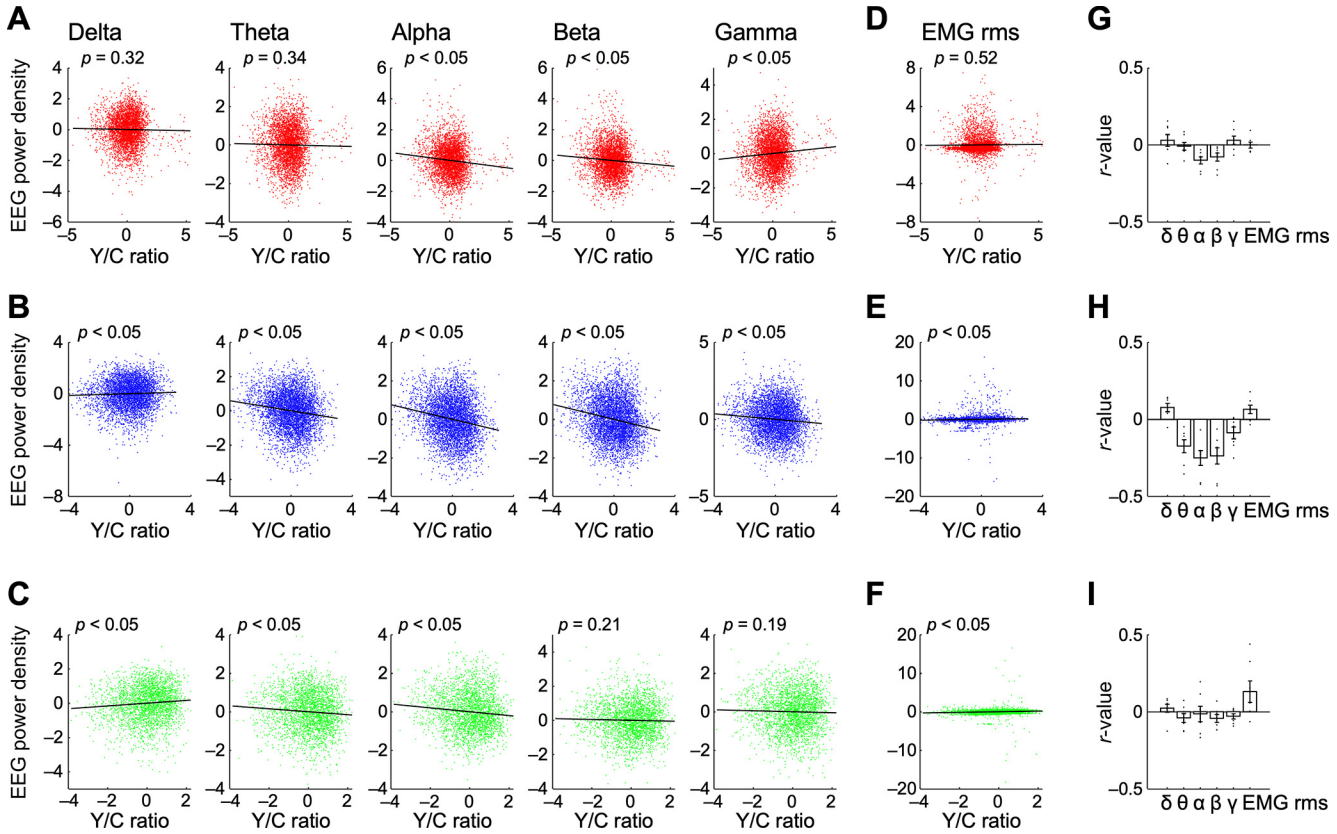

Figure 4. Correlation of EEG/EMG and cortical astrocyte Ca^{2+} signals during different sleep/wakefulness states. ***A–C***, Correlation analyses between normalized (z-scored) Y/C ratios from the cortex and normalized (z-scored) EEG power densities in the δ (1–5 Hz), θ (6–10 Hz), α (10–13 Hz), β (13–25 Hz), and γ (30–50 Hz) waves during wakefulness (***A***), NREM sleep (***B***), and REM sleep (***C***). ***D–F***, Correlation analyses between normalized Y/C ratios and normalized rms of EMG during wakefulness (***D***), NREM sleep (***E***), and REM sleep (***F***). The data in this figure were analyzed using 1-s bin sizes. ***G–I***, Bar graphs showing correlation coefficients summarizing the data from ***A–F***. The correlation coefficient of each recording was cross-validated by splitting the data into the first and second halves. Values are shown as means ± SEM.

in the hippocampus). In the hypothalamus and pons, however, episode duration of REM sleep and changes in Y/C ratios showed a significant negative correlation ($n = 11$ episodes from two recording sessions and one animal in the hypothalamus; $n = 5$ episodes from two recording sessions and one animal in the pons; $r = -0.67$, $p < 0.05$ in the hypothalamus; $r = -0.97$, $p < 0.05$ in the pons). These results suggest that the dynamics of astrocyte Ca^{2+} concentration vary depending on the brain region. A longer episode duration of REM sleep does not induce a further decrease in Ca^{2+} level in various regions of the brain, such as in the cortex and hippocampus.

Next, we analyzed the correlation between electrophysiological features from cortical EEGs and EMGs among the sleep/wakefulness states, and astrocyte Ca^{2+} concentrations, using the same methods as in Figure 2. As we compared cortical EEGs in this experiment, we focused on analyzing its correlation with the Ca^{2+} dynamics of cortical astrocytes (6 recording sessions and three animals). During wakefulness, Y/C ratios showed a weak negative correlation with α and β waves, and a weak positive correlation with γ waves (Fig. 4*A*,*D*,*G*). It was reported that an increase in the power value of δ and α waves and a decrease in the power value of γ waves indicate a decrease in the arousal level during wakefulness (McGinley et al., 2015). Cortical astrocyte Ca^{2+} levels appear to be low when mice are in quiet wakefulness. During NREM sleep, cortical Y/C ratios were positively correlated with δ waves, and were negatively correlated with θ, α, and β waves, consistent with those in the cerebellum (Fig. 4*B*, *E*,*H*). During REM sleep, however, Y/C ratios demonstrated a positive correlation with δ, and a negative correlation with θ and α waves (Fig. 4*C*,*F*,*I*). Although the Y scale has become too large to see the trend because of outliers, EMG power and Y/C ratio were positively correlated during both NREM and REM sleep (Fig. 4*E*,*F*). In this correlation analysis, minor but significant differences were observed also in the cerebellum. Compared with the results of the cerebellum, in the cortex, there was a tendency toward a correlation between astrocyte Ca^{2+} concentrations and electrophysiological features, not only during sleep but also during wakefulness.

Region-specific Ca^{2+} dynamics in astrocytes

We further quantified the regional differences in Ca^{2+} signals, including in the cerebellum. First, we quantified Ca^{2+} dynamics during each sleep/wakefulness episode, by categorizing the episodes into five states depending on the sleep/wakefulness state before and after each episode (Fig. 5*A*). Each episode was divided into five time-segments, and the average Ca^{2+} signal was calculated for each brain region ($n = 6$ recording sessions and three animals in the cortex; $n = 2$ recording sessions and one animal in the hippocampus; $n = 4$ recording sessions and two animals in the hypothalamus; $n = 2$ recording sessions and one animal in the pons; $n = 5$ recording sessions and three animals in the cerebellum).

Based on the results of Figures 3, 5*A*, there are likely to be three clusters in astrocyte Ca^{2+} signaling quality (Table 2). The first cluster is the cortex and hippocampus. Both cortical and hippocampal astrocytes showed a significant reduction in Ca^{2+}

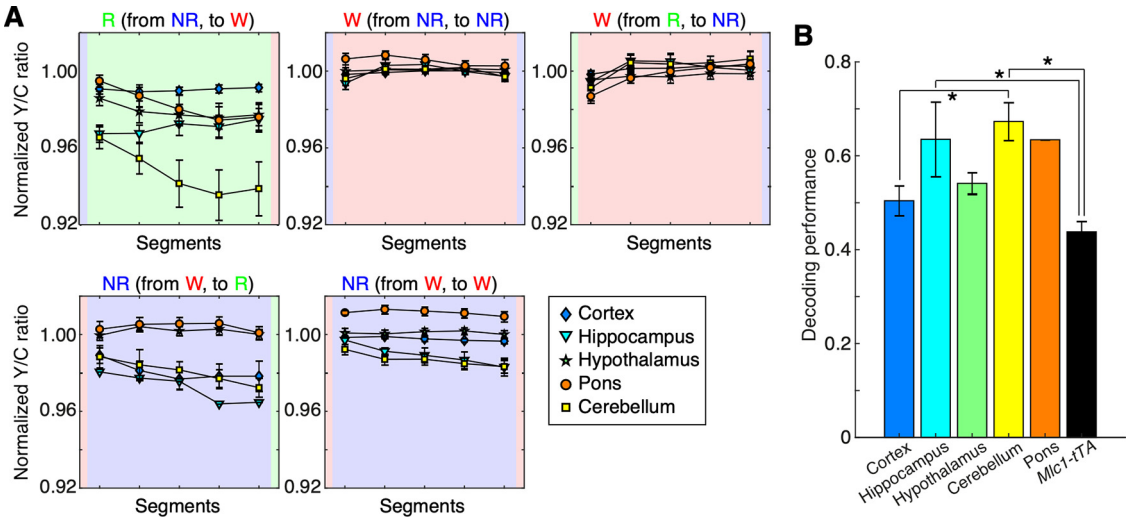

Figure 5. Dynamics of Ca^{2+} signals during different sleep/wakefulness states and different brain regions. ***A***, The mean profiles of Ca^{2+} signals during time-normalized episodes. In each panel, the duration of each episode was segmented into 5 bins and the mean normalized Y/C ratios were computed in various brain regions. ***B***, Decoding performance of Ca^{2+} signals for different sleep/wakefulness states among various brain regions; $*p < 0.05$, $F_{(5,17)} = 6.10$, one-way ANOVA with the *post hoc* HSD test. Values are shown as means ± SEM.

Table 2. Summary of region-specific and state-dependent astrocyte Ca^{2+} dynamics in mice

		Cortex	Hippocampus	Hypothalamus	Pons	Cerebellum
Normalized Y/C ratio	NR (vs W)	↓	↓	→	→	↓
	R (vs W)	↓	↓	↓	↓	↓
	R (vs NR)	↓	→	↓	↓	↓
State transition	W to NR	→	↓	→	→	↓
	NR to R	→	→	↓	↓	→
	NR to W	→	↑	→	→	↑
	R to W	↑	↑	↑	↑	↑
In episode	R (from NR, to W)	→	→	↓	↓	↓
	NR (from W, to R)	↓	↓	→	→	↓
Episode duration	R	→	→	↓	↓	↓

NR, NREM sleep; R, REM sleep; W, wakefulness.

concentration during NREM sleep. No significant change was observed during the state transition from NREM sleep to REM sleep. In addition, no correlation was observed between astrocyte Ca^{2+} concentration and the duration of REM sleep episodes. The second cluster is the hypothalamus and pons. Astrocytes of both regions maintained their Ca^{2+} concentrations during NREM sleep, which decreased during REM. The third cluster is the cerebellum. In addition, Ca^{2+} signals during the state transition and during REM sleep episodes were completely identical between the hypothalamus and pons. Cerebellar astrocytes include characteristics of the other two clusters, i.e., their Ca^{2+} changes associated with sleep/wakefulness states tend to resemble those of the cortex and hippocampus. However, as in the hypothalamus and brainstem, Ca^{2+} changes negatively correlated with the durations of REM episodes.

Next, we analyzed the extent to which astrocyte Ca^{2+} signals can predict the ongoing sleep/wakefulness state, and whether there are any differences in decoding performance among the brain regions. For this purpose, average Ca^{2+} signals were computed in each epoch, and a linear classifier was trained with four-fold cross validation (Tsunematsu et al., 2020). The decoding performance based on Y/C ratio of hippocampus and cerebellum in *Mlc1*-tTA; TetO-YCnano50 mice was significantly higher than that in *Mlc1*-tTA mice ($p < 0.05$, one-way ANOVA; Fig. 5*B*). This result indicates that hippocampal and cerebellar astrocyte activity demonstrate sleep/wakefulness state-dependency. In addition, we also clarified the differences in decoding performance among the different brain regions. Decoding performance of the cerebellum was significantly higher than that of the cortex ($p < 0.05$, one-way ANOVA; Fig. 5*B*). Thus, the physiological role of astrocytes in sleep/wakefulness might vary depending on the brain region.

Discussion

In the present study, we analyzed astrocyte Ca^{2+} dynamics during different sleep/wakefulness states among various brain regions. We demonstrated that astrocyte Ca^{2+} concentrations decreased during sleep, reached a minimum during REM sleep, and increased during wakefulness in all brain regions that were recorded. Further analyses indicated that there are at least three astrocyte clusters, comprising astrocytes from different brain regions. Although the association between changes in astrocyte Ca^{2+} concentrations and sleep/wakefulness were consistent in general among the brain regions, we found that detailed Ca^{2+} dynamics varies depending on the brain region.

Technical differences compared with other similar studies

Several recent studies measuring astrocyte Ca^{2+} concentrations during sleep/wakefulness states have been reported (Bojarskaite et al., 2020; Ingiosi et al., 2020). The results of these studies are in good agreement with our results showing that astrocyte Ca^{2+}

concentrations/signals decrease during sleep and increase during wakefulness. However, there are several differences. We showed a decrease in Ca^{2+} concentration in the cortex during NREM sleep, which is consistent with previous studies (Bojarskaite et al., 2020; Ingiosi et al., 2020). However, our present study demonstrated that no increase in Ca^{2+} level was observed during the transition from wakefulness to NREM sleep in the cortex, which is inconsistent with a recent study (Ingiosi et al., 2020). Moreover, both papers reported that the Ca^{2+} concentration once increased after transition from sleep to wakefulness then slightly decreased within 15 s. Our study, however, did not show a Ca^{2+} overshoot in any of the recorded brain regions, although we showed 32 s of data posttransition. These differences may be because of differences experimental conditions.

The first difference is the Ca^{2+} sensor that was used. We used the fluorescence resonance energy transfer-based, ultrasensitive genetically encoded Ca^{2+} indicator YCnano50 (Horikawa et al., 2010). On the other hand, other studies have used GCaMP6f (Chen et al., 2013). YCnano50 has high Ca^{2+} affinity (Kd = 50 nM) compared with GCaMP6f (Kd = 375 nM). Because of the ability of YCnano50 to detect subtle basal changes in the Ca^{2+} concentrations, our study was able to clarify the distinct differences in astrocyte Ca^{2+} concentrations between NREM and REM sleep.

The second difference is the method of expression of the Ca^{2+} sensor. Previous studies expressed the sensor using an adeno-associated virus, whereas we used *Mlc1*-tTA; TetO-YCnano50 bigenic mice to express the sensor in an astrocyte-specific manner. Because we used genetically modified mice rather than virus infection, the expression level and pattern of YCnano50 were constant among mice, and hence consistent data could be obtained. Although the sensors were substantially expressed in the cerebellum, pons, and hypothalamus, the sparce expression was observed in the cortex, and hippocampus in the genetically modified mice. It cannot exclude the possibility that the expression level of YCnano50 have made a difference from previous studies.

The third difference is the optical imaging approach that was used. As we recorded Ca^{2+} levels in astrocytes using the fiber photometry system, it was possible to analyze deeper regions of the brain, such as the hypothalamus and pons. However, our method only enables the measurement of the sum of changes in Ca^{2+} concentrations of cells. Our previous fiber photometry experiments using the same fiber optics and similar light intensities demonstrated that the detection limit is at a depth of ~700 μm (Natsubori et al., 2017). Assuming a tissue refractive index of 1.5, we detected signals with a diameter of ~800 μm at the 700 μm from tips of fiber optics. It indicates that the sum of Ca^{2+} signals of multiple nuclei and subregions were recorded although signals from specific brain region were detected at least. The Ca^{2+} dynamics at the nuclei, single-cell and subcellular level remains unknown. In recording from deep region, especially from the hypothalamus, the implanted optical fiber damaged the tissue and caused similar to glial scaring. Although there was no effect on the sleep/wakefulness state, the conclusion should be handled with care. Further detailed analyses are needed.

Nevertheless, taking advantage of our method, we succeeded in comparing astrocyte Ca^{2+} dynamics among various brain regions.

Correlation between electrophysiological features and astrocyte Ca^{2+} concentrations

Here, we investigated the correlation of cerebellar and cortical astrocyte Ca^{2+} concentrations with cortical oscillations. During NREM sleep, we found that consistent negative correlations between Y/C ratio and α/β power across recordings in the cerebellum and the cortex. Although β oscillations have long been implicated in long-range communication between brain regions (Fries, 2015), the function of such middle frequency oscillations during NREM sleep remains unclear. During REM sleep, we found negative correlations between Y/C ratio and θ power. Because θ power is a prominent biomarkers of REM sleep (Brown et al., 2012), astrocytic Ca^{2+} signals in the cortex and the cerebellum may reflect the depth and/or quality of REM sleep.

Possible mechanisms regulating astrocyte Ca^{2+} concentrations

We observed similar Ca^{2+} concentration changes in different brain regions. This was an interesting result that was inconsistent with neural activity. For instance, cortical neurons activate during wakefulness and REM sleep (Vyazovskiy et al., 2009; Watson et al., 2016; Niethard et al., 2017), hippocampal neurons fire less during REM sleep (Grosmark et al., 2012; Miyawaki and Diba, 2016), and an increase in the firing rate in the brainstem is observed during REM sleep (Hobson et al., 1975; Weber et al., 2015; Tsunematsu et al., 2020). Thus, it has been reported that neural activity patterns vary depending on the brain region.

It has also been reported that Ca^{2+} concentrations are affected by G-protein-coupled receptors (GPCRs) expressed in astrocytes via neurotransmitter release that accompanies neural activity. In general, the activation of astrocyte GPCRs increases astrocyte Ca^{2+} levels (Cornell-Bell et al., 1990; Takata et al., 2011; Jacob et al., 2014; Corkrum et al., 2020), although in some instances a decrease in Ca^{2+} level has been reported (Jennings et al., 2017). However, we observed global Ca^{2+} concentration changes, and therefore it is possible that a neurotransmitter that shows varying release patterns throughout the brain during different sleep/wakefulness states controls astrocyte Ca^{2+} concentration. Noradrenaline has been reported to increase astrocyte Ca^{2+} levels (Bekar et al., 2008; Paukert et al., 2014; Oe et al., 2020). Noradrenergic neurons located in the locus coeruleus project to the entire brain. Changes in firing rates of noradrenergic neurons showed a similar pattern to the Ca^{2+} dynamics of astrocytes (Takahashi et al., 2010; Tsujino et al., 2013). Taken together, noradrenaline released from noradrenergic neurons during wakefulness might increase astrocyte Ca^{2+} concentrations throughout the brain. In addition, considering that astrocyte Ca^{2+} levels gradually decrease during REM sleep, noradrenaline might also act as a volume transmitter, because microdialysis studies have reported that the concentration of noradrenaline in the brain decreases during sleep (Park, 2002; Bellesi et al., 2016). It has been reported that not only noradrenaline but also glutamate, acetylcholine, and GABA increase astrocyte Ca^{2+} levels (Cornell-Bell et al., 1990; Kang et al., 1998; Araque et al., 2002; Sun et al., 2013; Perea et al., 2016). Thus, the effects of these neurotransmitters as well as neuropeptides which regulate sleep/wakefulness state should be elucidated.

Possible heterogeneity of astrocytes among various brain regions

The results of this study surprisingly implicate that astrocytes in different brain regions may have different functions in sleep/wakefulness. Based on our results, we classified astrocytes into the following three clusters: cluster 1, astrocytes in the cortex and hippocampus; cluster 2, astrocytes in the hypothalamus and pons; and cluster 3, astrocytes in the cerebellum.

Astrocytes have recently been clarified to be a heterogeneous population. Transcriptional analyses have demonstrated that astrocyte gene expression patterns differ among and within brain regions and can be classified into several types (Chai et al., 2017; Zeisel et al., 2018; Batiuk et al., 2020; Bayraktar et al., 2020). The gene expression patterns indicated that cortical and hippocampal astrocytes have similar transcriptional profiles (Morel et al., 2017; Lozzi et al., 2020). In contrast, Bergmann glial cells are a type of cerebellar astrocyte with unique morphologic and transcriptional characteristics, although there are other glial cells, i.e., velate astrocytes, in the cerebellum. Bergmann glial cells express Ca^{2+}-permeable AMPA receptors composed of the GluA1 and GluA4 subunits (Saab et al., 2012), implying that they have different intracellular Ca^{2+} dynamics. Our results may explain part of the differences in the functions of astrocytes depending on the brain region, as well as the differences in their cellular transcriptomes. In our study, the number of mice in which the hippocampus and pons was analyzed was limited, although the effect size was 1.34 and 1.13, respectively. Furthermore, the effect size calculated from the data of the cortex was 0.47, indicating a medium effect. Thus, further analyses are required before making any definite conclusions.

Decoding performance for ongoing sleep/wakefulness states was significantly higher in the hippocampus and cerebellum of *Mlc1*-tTA; TetO-YCnano50 mice than *Mlc1*-tTA mice, suggesting that astrocyte Ca^{2+} dynamics might not only show state-dependent fluctuation, but also contribute to the control of the sleep/wakefulness state itself. Further research should be performed with the caveat that astrocyte functions in sleep/wakefulness states might vary among different brain regions.

References

Allen NJ (2014) Astrocyte regulation of synaptic behavior. Annu Rev Cell Dev Biol 30:439–463.

Allen NJ, Eroglu C (2017) Cell biology of astrocyte-synapse interactions. Neuron 96:697–708.

Araque A, Martín ED, Perea G, Arellano JI, Buño W (2002) Synaptically released acetylcholine evokes Ca2+ elevations in astrocytes in hippocampal slices. J Neurosci 22:2443–2450.

Araque A, Carmignoto G, Haydon PG, Oliet SH, Robitaille R, Volterra A (2014) Gliotransmitters travel in time and space. Neuron 81:728–739.

Batiuk MY, Martirosyan A, Wahis J, de Vin F, Marneffe C, Kusserow C, Koeppen J, Viana JF, Oliveira JF, Voet T, Ponting CP, Belgard TG, Holt MG (2020) Identification of region-specific astrocyte subtypes at single cell resolution. Nat Commun 11:1220.

Bayraktar OA, Bartels T, Holmqvist S, Kleshchevnikov V, Martirosyan A, Polioudakis D, Ben Haim L, Young AMH, Batiuk MY, Prakash K, Brown A, Roberts K, Paredes MF, Kawaguchi R, Stockley JH, Sabeur K, Chang SM, Huang E, Hutchinson P, Ullian EM, et al. (2020) Astrocyte layers in the mammalian cerebral cortex revealed by a single-cell in situ transcriptomic map. Nat Neurosci 23:500–509.

Bekar LK, He W, Nedergaard M (2008) Locus coeruleus alpha-adrenergic-mediated activation of cortical astrocytes in vivo. Cereb Cortex 18:2789–2795.

Bellesi M, Tononi G, Cirelli C, Serra PA (2016) Region-specific dissociation between cortical noradrenaline levels and the sleep/wake cycle. Sleep 39:143–154.

Beppu K, Sasaki T, Tanaka KF, Yamanaka A, Fukazawa Y, Shigemoto R, Matsui K (2014) Optogenetic countering of glial acidosis suppresses glial glutamate release and ischemic brain damage. Neuron 81:314–320.

Bojarskaite L, Bjørnstad DM, Pettersen KH, Cunen C, Hermansen GH, Åbjørsbråten KS, Chambers AR, Sprengel R, Vervaeke K, Tang W, Enger R, Nagelhus EA (2020) Astrocytic Ca(2+) signaling is reduced during sleep and is involved in the regulation of slow wave sleep. Nat Commun 11:3240.

Boor PK, de Groot K, Waisfisz Q, Kamphorst W, Oudejans CB, Powers JM, Pronk JC, Scheper GC, van der Knaap MS (2005) MLC1: a novel protein in distal astroglial processes. J Neuropathol Exp Neurol 64:412–419.

Brown RE, Basheer R, McKenna JT, Strecker RE, McCarley RW (2012) Control of Sleep and Wakefulness. Physiol Rev 92:1087–1187.

Chai H, Diaz-Castro B, Shigetomi E, Monte E, Octeau JC, Yu X, Cohn W, Rajendran PS, Vondriska TM, Whitelegge JP, Coppola G, Khakh BS (2017) Neural circuit-specialized astrocytes: transcriptomic, proteomic, morphological, and functional evidence. Neuron 95:531–549.e9.

Chen TW, Wardill TJ, Sun Y, Pulver SR, Renninger SL, Baohan A, Schreiter ER, Kerr RA, Orger MB, Jayaraman V, Looger LL, Svoboda K, Kim DS (2013) Ultrasensitive fluorescent proteins for imaging neuronal activity. Nature 499:295–300.

Clasadonte J, Scemes E, Wang Z, Boison D, Haydon PG (2017) Connexin 43-mediated astroglial metabolic networks contribute to the regulation of the sleep-wake cycle. Neuron 95:1365–1380.e5.

Corkrum M, Covelo A, Lines J, Bellocchio L, Pisansky M, Loke K, Quintana R, Rothwell PE, Lujan R, Marsicano G, Martin ED, Thomas MJ, Kofuji P, Araque A (2020) Dopamine-evoked synaptic regulation in the nucleus accumbens requires astrocyte activity. Neuron 105:1036–1047. e1035.

Cornell-Bell AH, Finkbeiner SM, Cooper MS, Smith SJ (1990) Glutamate induces calcium waves in cultured astrocytes: long-range glial signaling. Science 247:470–473.

Faul F, Erdfelder E, Lang AG, Buchner A (2007) G*Power 3: a flexible statistical power analysis program for the social, behavioral, and biomedical sciences. Behav Res Methods 39:175–191.

Filosa JA, Naskar K, Perfume G, Iddings JA, Biancardi VC, Vatta MS, Stern JE (2012) Endothelin-mediated calcium responses in supraoptic nucleus astrocytes influence magnocellular neurosecretory firing activity. J Neuroendocrinol 24:378–392.

Florian C, Vecsey CG, Halassa MM, Haydon PG, Abel T (2011) Astrocyte-derived adenosine and A1 receptor activity contribute to sleep loss-induced deficits in hippocampal synaptic plasticity and memory in mice. J Neurosci 31:6956–6962.

Frank MG (2019) The role of glia in sleep regulation and function. Handb Exp Pharmacol 253:83–96.

Fries P (2015) Rhythms for cognition: communication through coherence. Neuron 88:220–235.

Gourine AV, Kasymov V, Marina N, Tang F, Figueiredo MF, Lane S, Teschemacher AG, Spyer KM, Deisseroth K, Kasparov S (2010) Astrocytes control breathing through pH-dependent release of ATP. Science 329:571–575.

Grosmark AD, Mizuseki K, Pastalkova E, Diba K, Buzsáki G (2012) REM sleep reorganizes hippocampal excitability. Neuron 75:1001–1007.

Halassa MM, Florian C, Fellin T, Munoz JR, Lee S-Y, Abel T, Haydon PG, Frank MG (2009) Astrocytic modulation of sleep homeostasis and cognitive consequences of sleep loss. Neuron 61:213–219.

Hayashi Y, Kashiwagi M, Yasuda K, Ando R, Kanuka M, Sakai K, Itohara S (2015) Cells of a common developmental origin regulate REM/non-REM sleep and wakefulness in mice. Science 350:957–962.

Hobson JA, McCarley RW, Wyzinski PW (1975) Sleep cycle oscillation: reciprocal discharge by two brainstem neuronal groups. Science 189:55–58.

Holmström KM, Marina N, Baev AY, Wood NW, Gourine AV, Abramov AY (2013) Signalling properties of inorganic polyphosphate in the mammalian brain. Nat Commun 4:1362.

Hoogland TM, Kuhn B, Gobel W, Huang W, Nakai J, Helmchen F, Flint J, Wang SS (2009) Radially expanding transglial calcium waves in the intact cerebellum. Proc Natl Acad Sci USA 106:3496–3501.

Horikawa K, Yamada Y, Matsuda T, Kobayashi K, Hashimoto M, Matsu-ura T, Miyawaki A, Michikawa T, Mikoshiba K, Nagai T (2010) Spontaneous network activity visualized by ultrasensitive Ca(2+) indicators, yellow cameleon-nano. Nat Methods 7:729–732.

Ingiosi AM, Hayworth CR, Harvey DO, Singletary KG, Rempe MJ, Wisor JP, Frank MG (2020) A role for astroglial calcium in mammalian sleep and sleep regulation. Curr Biol 30:4373–4383.e7.

Jacob PF, Vaz SH, Ribeiro JA, Sebastião AM (2014) P2Y1 receptor inhibits GABA transport through a calcium signalling-dependent mechanism in rat cortical astrocytes. Glia 62:1211–1226.

Jennings A, Tyurikova O, Bard L, Zheng K, Semyanov A, Henneberger C, Rusakov DA (2017) Dopamine elevates and lowers astroglial Ca(2+) through distinct pathways depending on local synaptic circuitry. Glia 65:447–459.

Kanemaru K, Sekiya H, Xu M, Satoh K, Kitajima N, Yoshida K, Okubo Y, Sasaki T, Moritoh S, Hasuwa H, Mimura M, Horikawa K, Matsui K, Nagai T, Iino M, Tanaka KF (2014) In vivo visualization of subtle, transient, and local activity of astrocytes using an ultrasensitive Ca(2+) indicator. Cell Rep 8:311–318.

Kang J, Jiang L, Goldman SA, Nedergaard M (1998) Astrocyte-mediated potentiation of inhibitory synaptic transmission. Nat Neurosci 1:683–692.

Liu D, Dan Y (2019) A motor theory of sleep-wake control: arousal-action circuit. Annu Rev Neurosci 42:27–46.

Lozzi B, Huang TW, Sardar D, Huang AY, Deneen B (2020) Regionally distinct astrocytes display unique transcription factor profiles in the adult brain. Front Neurosci 14:61.

Magistretti PJ, Allaman I (2018) Lactate in the brain: from metabolic end-product to signalling molecule. Nat Rev Neurosci 19:235–249.

McGinley MJ, Vinck M, Reimer J, Batista-Brito R, Zagha E, Cadwell CR, Tolias AS, Cardin JA, McCormick DA (2015) Waking state: rapid variations modulate neural and behavioral responses. Neuron 87:1143–1161.

Min R, Nevian T (2012) Astrocyte signaling controls spike timing-dependent depression at neocortical synapses. Nat Neurosci 15:746–753.

Miyawaki H, Diba K (2016) Regulation of hippocampal firing by network oscillations during sleep. Curr Biol 26:893–902.

Morel L, Chiang MSR, Higashimori H, Shoneye T, Iyer LK, Yelick J, Tai A, Yang Y (2017) Molecular and functional properties of regional astrocytes in the adult brain. J Neurosci 37:8706–8717.

Natsubori A, Tsutsui-Kimura I, Nishida H, Bouchekioua Y, Sekiya H, Uchigashima M, Watanabe M, de Kerchove d'Exaerde A, Mimura M, Takata N, Tanaka KF (2017) Ventrolateral striatal medium spiny neurons positively regulate food-incentive, goal-directed behavior independently of D1 and D2 selectivity. J Neurosci 37:2723–2733.

Navarrete M, Araque A (2010) Endocannabinoids potentiate synaptic transmission through stimulation of astrocytes. Neuron 68:113–126.

Niethard N, Burgalossi A, Born J (2017) Plasticity during sleep is linked to specific regulation of cortical circuit activity. Front Neural Circuits 11:65.

Nimmerjahn A, Mukamel EA, Schnitzer MJ (2009) Motor behavior activates Bergmann glial networks. Neuron 62:400–412.

Oe Y, Wang X, Patriarchi T, Konno A, Ozawa K, Yahagi K, Hirai H, Tsuboi T, Kitaguchi T, Tian L, McHugh TJ, Hirase H (2020) Distinct temporal integration of noradrenaline signaling by astrocytic second messengers during vigilance. Nat Commun 11:471.

Park SP (2002) In vivo microdialysis measures of extracellular norepinephrine in the rat amygdala during sleep-wakefulness. J Korean Med Sci 17:395–399.

Paukert M, Agarwal A, Cha J, Doze VA, Kang JU, Bergles DE (2014) Norepinephrine controls astroglial responsiveness to local circuit activity. Neuron 82:1263–1270.

Pelluru D, Konadhode RR, Bhat NR, Shiromani PJ (2016) Optogenetic stimulation of astrocytes in the posterior hypothalamus increases sleep at night in C57BL/6J mice. Eur J Neurosci 43:1298–1306.

Perea G, Gómez R, Mederos S, Covelo A, Ballesteros JJ, Schlosser L, Hernández-Vivanco A, Martín-Fernández M, Quintana R, Rayan A, Díez A, Fuenzalida M, Agarwal A, Bergles DE, Bettler B, Manahan-Vaughan D, Martín ED, Kirchhoff F, Araque A (2016) Activity-dependent switch of GABAergic inhibition into glutamatergic excitation in astrocyte-neuron networks. Elife 5:e20362.

Poskanzer KE, Yuste R (2016) Astrocytes regulate cortical state switching in vivo. Proc Natl Acad Sci USA 113:E2675–E2684.

Radulovacki M, Virus RM, Djuricic-Nedelson M, Green RD (1984) Adenosine analogs and sleep in rats. J Pharmacol Exp Ther 228:268–274.

Saab AS, Neumeyer A, Jahn HM, Cupido A, Simek AA, Boele HJ, Scheller A, Le Meur K, Gotz M, Monyer H, Sprengel R, Rubio ME, Deitmer JW, De Zeeuw CI, Kirchhoff F (2012) Bergmann glial AMPA receptors are required for fine motor coordination. Science 337:749–753.

Sakurai T (2007) The neural circuit of orexin (hypocretin): maintaining sleep and wakefulness. Nat Rev Neurosci 8:171–181.

Sasaki T, Beppu K, Tanaka KF, Fukazawa Y, Shigemoto R (2012) Application of an optogenetic byway for perturbing neuronal activity via glial photostimulation. Proc Natl Acad Sci USA 109:20720–20725.

Savtchouk I, Volterra A (2018) Gliotransmission: beyond Black-and-White. J Neurosci 38:14–25.

Scammell TE, Arrigoni E, Lipton JO (2017) Neural circuitry of wakefulness and sleep. Neuron 93:747–765.

Sofroniew MV, Vinters HV (2010) Astrocytes: biology and pathology. Acta Neuropathol 119:7–35.

Srinivasan R, Huang BS, Venugopal S, Johnston AD, Chai H, Zeng H, Golshani P, Khakh BS (2015) Ca(2+) signaling in astrocytes from Ip3r2 (-/-) mice in brain slices and during startle responses in vivo. Nat Neurosci 18:708–717.

Sun W, McConnell E, Pare JF, Xu Q, Chen M, Peng W, Lovatt D, Han X, Smith Y, Nedergaard M (2013) Glutamate-dependent neuroglial calcium signaling differs between young and adult brain. Science 339:197–200.

Takahashi K, Kayama Y, Lin JS, Sakai K (2010) Locus coeruleus neuronal activity during the sleep-waking cycle in mice. Neuroscience 169:1115–1126.

Takata N, Mishima T, Hisatsune C, Nagai T, Ebisui E, Mikoshiba K, Hirase H (2011) Astrocyte calcium signaling transforms cholinergic modulation to cortical plasticity in vivo. J Neurosci 31:18155–18165.

Tanaka KF, Ahmari SE, Leonardo ED, Richardson-Jones JW, Budreck EC, Scheiffele P, Sugio S, Inamura N, Ikenaka K, Hen R (2010) Flexible accelerated STOP tetracycline operator-knockin (FAST): a versatile and efficient new gene modulating system. Biol Psychiatry 67:770–773.

Tanaka KF, Matsui K, Sasaki T, Sano H, Sugio S, Fan K, Hen R, Nakai J, Yanagawa Y, Hasuwa H, Okabe M, Deisseroth K, Ikenaka K, Yamanaka A (2012) Expanding the repertoire of optogenetically targeted cells with an enhanced gene expression system. Cell Rep 2:397–406.

Teijido O, Casaroli-Marano R, Kharkovets T, Aguado F, Zorzano A, Palacín M, Soriano E, Martínez A, Estévez R (2007) Expression patterns of MLC1 protein in the central and peripheral nervous systems. Neurobiol Dis 26:532–545.

Thrane AS, Thrane VR, Zeppenfeld D, Lou N, Xu Q, Nagelhus E, Nedergaard M (2012) General anesthesia selectively disrupts astrocyte calcium signaling in the awake mouse cortex. Proc Natl Acad Sci USA 109:18974–18979.

Tobler I, Deboer T, Fischer M (1997) Sleep and sleep regulation in normal and prion protein-deficient mice. J Neurosci 17:1869–1879.

Tsujino N, Tsunematsu T, Uchigashima M, Konno K, Yamanaka A, Kobayashi K, Watanabe M, Koyama Y, Sakurai T (2013) Chronic alterations in monoaminergic cells in the locus coeruleus in orexin neuron-ablated narcoleptic mice. PLoS One 8:e70012.

Tsunematsu T, Ueno T, Tabuchi S, Inutsuka A, Tanaka KF, Hasuwa H, Kilduff TS, Terao A, Yamanaka A (2014) Optogenetic manipulation of activity and temporally controlled cell-specific ablation reveal a role for MCH neurons in sleep/wake regulation. J Neurosci 34:6896–6909.

Tsunematsu T, Patel AA, Onken A, Sakata S (2020) State-dependent brainstem ensemble dynamics and their interactions with hippocampus across sleep states. Elife 9:e52244.

Tsutsui-Kimura I, Natsubori A, Mori M, Kobayashi K, Drew MR, de Kerchove d'Exaerde A, Mimura M, Tanaka KF (2017) Distinct roles of ventromedial versus ventrolateral striatal medium spiny neurons in reward-oriented behavior. Curr Biol 27:3042–3048.e4.

Vyazovskiy VV, Olcese U, Lazimy YM, Faraguna U, Esser SK, Williams JC, Cirelli C, Tononi G (2009) Cortical firing and sleep homeostasis. Neuron 63:865–878.

Watson BO, Levenstein D, Greene JP, Gelinas JN (2016) Network homeostasis and state dynamics of neocortical sleep. Neuron 90:839–852.

Weber F, Dan Y (2016) Circuit-based interrogation of sleep control. Nature 538:51–59.

Weber F, Chung S, Beier KT, Xu M, Luo L, Dan Y (2015) Control of REM sleep by ventral medulla GABAergic neurons. Nature 526:435–438.

Xie L, Kang H, Xu Q, Chen MJ, Liao Y, Thiyagarajan M, O'Donnell J, Christensen DJ, Nicholson C, Iliff JJ, Takano T, Deane R, Nedergaard M (2013) Sleep drives metabolite clearance from the adult brain. Science 342:373–377.

Yoshida K, Tsutsui-Kimura I, Kono A, Yamanaka A, Kobayashi K, Watanabe M, Mimura M, Tanaka KF (2020) Opposing ventral striatal medium spiny neuron activities shaped by striatal parvalbumin-expressing interneurons during goal-directed behaviors. Cell Rep 31:107829.

Zeisel A, Hochgerner H, Lönnerberg P, Johnsson A, Memic F, van der Zwan J, Häring M, Braun E, Borm LE, La Manno G, Codeluppi S, Furlan A, Lee K, Skene N, Harris KD, Hjerling-Leffler J, Arenas E, Ernfors P, Marklund U, Linnarsson S (2018) Molecular architecture of the mouse nervous system. Cell 174:999–1014.e22.